

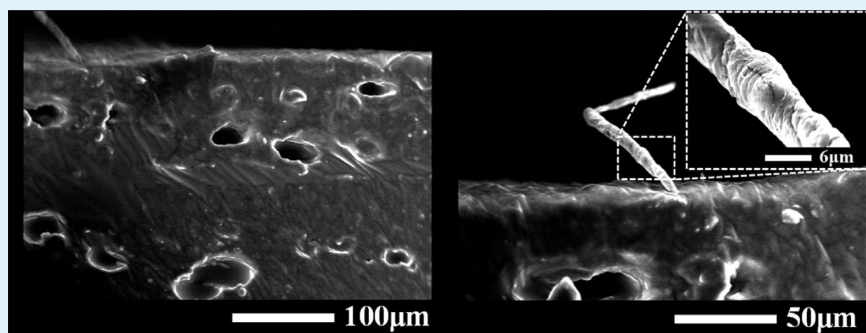
# Hybrid Self-Healing Matrix Using Core–Shell Nanofibers and Capsuleless Microdroplets

Min Wook Lee,<sup>†,‡</sup> Seongpil An,<sup>†,‡</sup> Changmin Lee,<sup>†,§</sup> Minh Liou,<sup>†</sup> Alexander L. Yarin,<sup>\*,†,||</sup> and Sam S. Yoon<sup>\*,†</sup>

<sup>†</sup>School of Mechanical Engineering, <sup>§</sup>Green School, and <sup>†</sup>College of Engineering, Korea University, Seoul 136-713, Republic of Korea

<sup>||</sup>Department of Mechanical and Industrial Engineering, University of Illinois at Chicago, Chicago, Illinois 60607-7022, United States

## S Supporting Information



**ABSTRACT:** In this work, we developed novel self-healing anticorrosive hierarchical coatings that consist of several components. Namely, as a skeleton we prepared a core–shell nanofiber mat electrospun from emulsions of cure material (dimethyl methylhydrogen siloxane) in a poly(acrylonitrile) (PAN) solution in dimethylformamide. In these nanofibers, cure is in the core, while PAN is in the shell. The skeleton deposited on a protected surface is encased in an epoxy-based matrix, which contains emulsified liquid droplets of dimethylvinyl-terminated dimethylsiloxane resin monomer. When such hierarchical coatings are damaged, cure is released from the nanofiber cores and the resin monomer, released from the damaged matrix, is polymerized in the presence of cure. This polymerization and solidification process takes about 1–2 days and eventually heals the damaged material when solid poly(dimethylsiloxane) resin is formed. The self-healing effect was demonstrated using an electrochemical analogue of the scanning vibrating electrode technique. Damaged samples were left for 2 days. After that, the electric current through a damaged coating was found to be negligibly small for the samples with self-healing properties. On the other hand, for the samples without self-healing properties, the electric current was significant.

**KEYWORDS:** self-healing, core–shell nanofibers, electrospinning, emulsions

## 1. INTRODUCTION

Composites have been known to have high mechanical strength but be light in weight; therefore, they have been considered as an ideal material for numerous applications that call for high structural reliability and low payload.<sup>1–3</sup> For this reason, composites have been used in various industries including automobile, aerospace, and robotics as well as in medicine. In general, composite materials consist of multiple layers of fiber-reinforced structures whose tensile strength reaches from tens to hundreds of megapascals.<sup>2,3</sup> Despite this superior mechanical strength, the materials possess a fatal weakness in the transversal direction into which the composite layers are stuck and glued together. When a composite is subject to damage due to a transversal load, interlayer microcracks grow, which eventually delaminates the composite. This delamination eventually leads to catastrophic failure of the structure. The microcracks developed due to a steady-state load or fatigue are difficult to detect and repair because these microcracks grow inside the structure over a long period of time. For this reason,

an autonomous “self-healing” self-entangled nanofiber layer that “detects” and repairs these microcracks would be ideal from both technological and economical perspectives. Such a self-healing capability would mimic, in a certain sense, the self-healing in biology and nature.<sup>4</sup>

In this study, poly(dimethylsiloxane) (PDMS) is used as a healing agent, which is the final product of resin and cure. The cure material was emulsified and electrospun inside a nanofiber, as depicted in Figure 1. Resin was also prepared as emulsified droplets inside epoxy and later poured into a matrix (which consists of both cure nanofibers and resin-embedded epoxy), which later solidifies. Resin also could have been stored inside a nanofiber. However, in general, the required amount of resin with respect to that of cure is about 10:1 to yield mechanically and structurally reliable PDMS. This requirement of high

Received: April 3, 2014

Accepted: June 2, 2014

Published: June 2, 2014

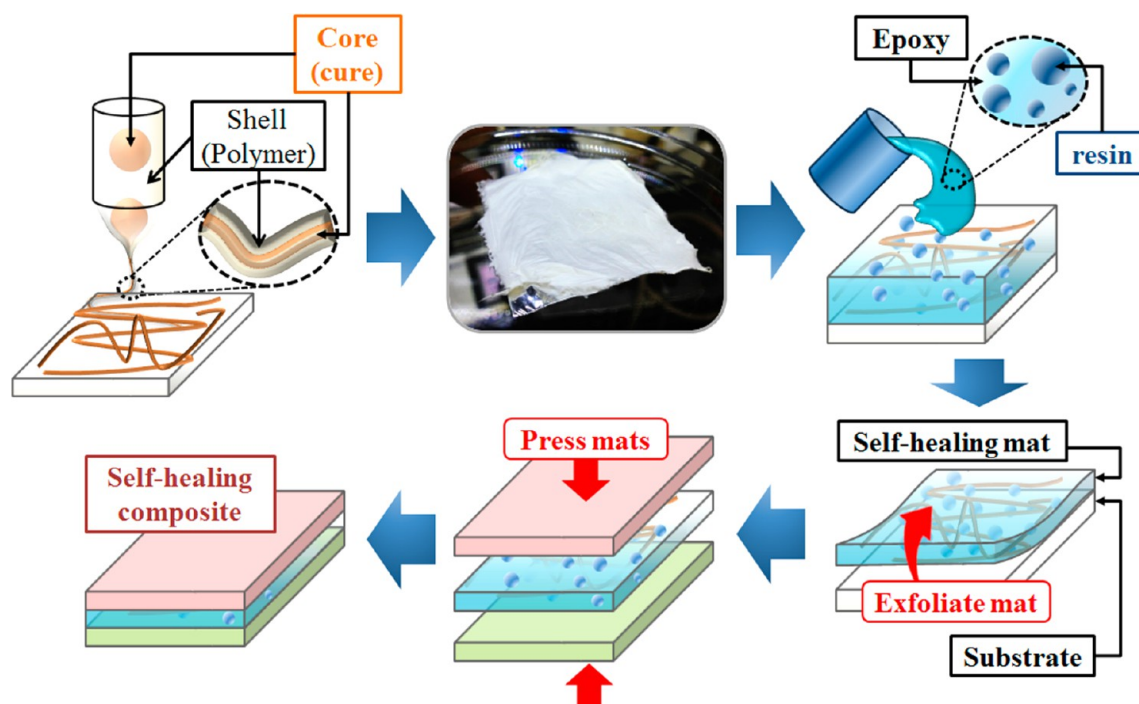


**Figure 1.** Schematic of the solution electrospinning of core-shell nanofibers (on the left) and encasing them in an epoxy-resin emulsion to prepare a self-healing composite.

volume ratio inflicts a heavy burden on the production of resin nanofibers. For this reason, we prepared resin as emulsion droplets inside epoxy, which can accommodate a sufficient amount of resin. When epoxy solidifies, the emulsion droplets are firmly trapped inside the solidified epoxy.

This capsuleless approach eliminates the inconvenience of manufacturing microcapsules. It is worth noting that capsule production is complex and expensive and involves solvent evaporation, vacuum filtration, cleaning, drying, and other procedures.<sup>5–11</sup> Moreover, the final product has a thick shell or capsule, which is waste once capsules are fractured.<sup>12</sup> In addition, it is desirable to minimize the volume occupied by capsules for structural stability. For this reason, we have adopted the capsuleless approach for resin and the core-shell nanofibers for cure. In this approach, we efficiently control the amount of resin, while retaining the 3D nanofiber network.

## 2. EXPERIMENTAL SECTION

In this study, a platinum-catalyst-contained dimethylvinyl-terminated dimethylsiloxane (DMS) resin monomer and an appropriate cure are used in the healing process. The cure material dimethyl methylhydrogen siloxane (DMHS) was emulsified in poly(acrylonitrile) (PAN) and electrospun as core-shell nanofibers, with cure being in the core and PAN in the shell, as depicted in Figure 1. In addition, an emulsion of DMS resin monomer droplets in epoxy was prepared and later poured into an as-spun nanofiber matrix. The resulting material, composed of both cure-containing nanofibers and resin-containing epoxy, was left to solidify, which is called a “matrix”. On the other hand, DMS resin could also have been encapsulated in the nanofiber core, which we did not adopt because the approach would require an equal amount of DMS and cure. Indeed, the optimal curing reaction stoichiometry requires 10 times more DMS resin than cure, a requirement that is difficult to meet if resin is brought into the nanofiber cores.<sup>13</sup> Therefore, it is preferable to deliver cure in the nanofiber core while dispersing a sufficient amount of DMS resin in the epoxy matrix, as sketched in Figure 1. Furthermore, we herein adopted the current approach because the emulsified resin micro-

droplets inside epoxy are spherical and do not require any shell. When epoxy solidifies, it encapsulates and preserves the resin droplets. The resin monomer is polymerized in the presence of cure to form PDMS resin when both were released from the droplets and nanofibers, respectively, when material was fractured.

**2.1. Cure-Containing Nanofibers.** Using the emulsion electrospinning,<sup>14,15</sup> core-shell nanofibers containing DMHS (cure) were electrospun from the cure-DMHS solution in a PAN-dimethylformamide (DMF) solution onto substrates:  $2.5 \times 2.5 \text{ cm}^2$  indium-tin oxide (ITO) substrates for a transmittance test and  $2 \times 2 \text{ cm}^2$  stainless steel substrates for an electrochemical test.

The cure droplets were dispersed in an 8 wt % PAN ( $M_w = 150 \text{ kDa}$ ) solution in DMF, denoted as PAN-DMF. Being electrospun from a single nozzle, such an emulsion forms core-shell fibers with cure in the core and a PAN-DMF matrix in the shell. The weight ratio of the core-to-shell materials was 1:5. The resulting emulsion was mixed for 24 h using a magnetic stirrer. To refine the emulsified droplets, the emulsion was sonicated for 15 s, which was repeated eight times, so that the total sonication time was about 2 min. Because the emulsion was metastable, it was electrospun within 1 h after preparation. The flow rate of the emulsion solution was in the range of  $400 \mu\text{L/h} < Q < 500 \mu\text{L/h}$ . The voltage applied to the needle was in the range of  $7 \text{ kV} < V < 8.6 \text{ kV}$ . The standoff distance between the nozzle and substrate was 7 cm. The inner and outer diameters of the nozzle were 0.84 and 1.27 mm, respectively. The duration of electrospinning was  $t_{\text{dep}} = 3$  and 10 min, which varied the amount of cure in the as-spun nanofiber mat. It is worth noting that the amount of cure can also be controlled by varying the cure concentration, flow rate, and standoff distance. However, we herein chose the deposition time as a parameter controlling the cure amount.

**2.2. Epoxy-Resin Emulsion.** The epoxy-resin emulsion was prepared by mixing 5, 10, and 20 wt % resin with respect to the weight of epoxy (Evergreen Pro, Samhwa Paint), as sketched in Figure 1. The epoxy-resin emulsion was milky and turbid, with resin being the dispersed phase and epoxy the continuous phase. To fragment the resin drops in the emulsion into finer droplets, it was sonicated for 2 min using an ultrasonicator (Q700; Qsonica, Newtown, CT). The temperature of the emulsion ( $70 \text{ }^\circ\text{C}$ ) was monitored so it did not exceed the boiling temperature of the solvent DMF ( $T_b \sim 154 \text{ }^\circ\text{C}$ ).

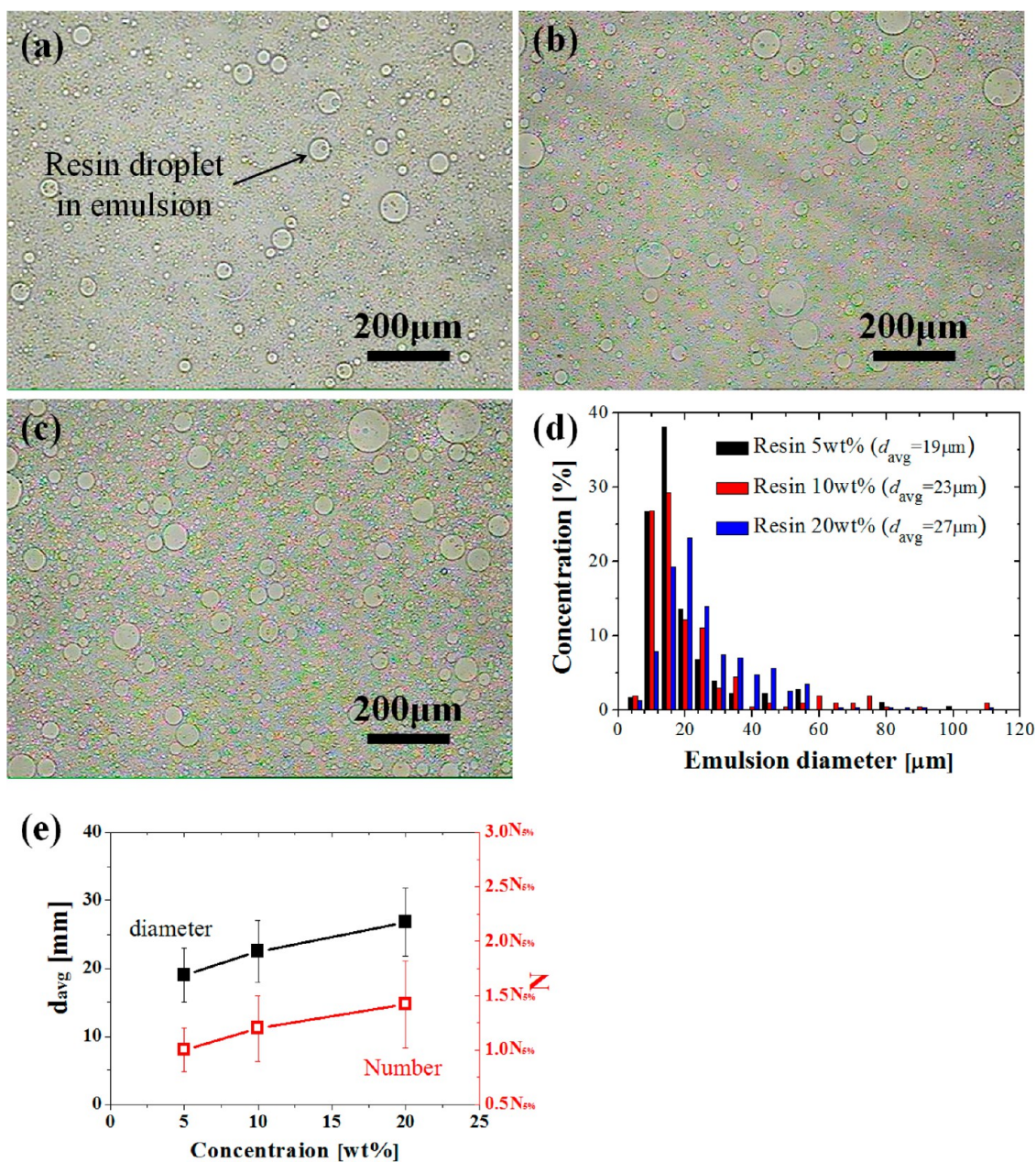


**Figure 2.** Emulsion OM images: (a) 5 wt % resin; (b) 10 wt % resin; (c) 20 wt % resin. (d) Size distribution. (e) Emulsion drop average diameter and the number of drops in the emulsion.

Emulsion preparation was conducted in an open atmosphere at room temperature. As a final step, the epoxy–resin emulsion was poured onto a core–shell cure-containing nanofiber mat. About 24 h was given to solidify the epoxy–resin layer. It should be emphasized that when nanofibers are embedded, epoxy spreads because of wettability. If in such a process significant tractions were developed and nanofibers broken, cure would be released and polymerize resin, which would immediately arrest the epoxy spreading. Because the spreading proceeds, nanofibers are not broken.

**2.3. Characterizations.** All scanning electron microscopy (SEM) images were obtained using a S-5000 microscope (Hitachi, Ltd.). The electrospinning process was monitored by a high-speed camera (Phantom 9.1, Vision Research Inc.) at a frame rate of  $\sim 2000$  fps with LED lighting (50 W). The optical images of the emulsion structure at different resin per varying concentration were obtained using an optical microscope in refraction mode with a magnification of  $100\times$ . To evaluate transmittance of the self-healing composite deposited on a

transparent flexible ITO substrate ( $2.5 \times 2.5 \times 0.07 \text{ cm}^3$ ), a UV–vis spectrophotometer (Optizen POP) was used.

The relative amounts of pure epoxy, nanofiber mat with cure, and resin at different concentrations in the self-healing composite were evaluated using thermogravimetry (TGA) and differential thermogravimetry (DTG) analyses. For that purpose, the composite samples ( $\sim 3 \text{ mg}$ ) were collected onto a pan-type holder with a diameter of 7 mm. The holder was sealed by a cap, and the sample was pressed. The TGA and DTG analyses were conducted (2050 TGA; TA Instruments) under a nitrogen atmosphere with a heating rate of  $10 \text{ }^\circ\text{C}/\text{min}$  in the temperature range of  $30 \text{ }^\circ\text{C} < T < 800 \text{ }^\circ\text{C}$ .

Because the current self-healing composite is not transparent, an electrochemical analogue device known as scanning vibrating electrode technique (SVET) was used. Once a cut is made to the coating, the bottom stainless steel is exposed to the electrolyte. The electric current in the circuit becomes possible when the coating layer is not self-healed. On the other hand, self-healing would insulate the stainless steel surface and, thus, eliminate the current. The electrolyte used was

a 1 M NaCl aqueous solution. The electric current was recorded as a function of time by a sourcemeter (Keithley 2400). The bias voltage applied was 3 V, the compliance limit was 1 A, and the measurement lasted for 200 s. The viscosity of emulsion solutions was measured by a viscometer (LV DV-I+CP, Brookfield) at room temperature.

### 3. RESULTS AND DISCUSSION

**3.1. Resin–Epoxy Emulsion Solution.** The optical microscopy (OM) images of the resin–epoxy emulsion solution at several resin concentrations (5, 10, and 20 wt %) are shown in Figure 2. The resin droplets in the emulsions are perfectly spherical. At least 10 OM images were used to measure a statistically sound droplet-size distribution and the average droplet size. It was found that the larger the resin concentration in the emulsion, the larger are the resin droplets. The average diameters of these resin droplets were 19, 23, and 27  $\mu\text{m}$  for 5, 10, and 20 wt %, respectively, as shown in Figure 2d.

In Figure 2e, the average drop diameter versus concentration is shown. The number of drops  $N$  increased with the resin concentration (Figure 2e). In particular, for a 5–10 wt % concentration increase, nearly a 20% increase in the number of resin droplets was observed compared to the initial droplet number,  $N_{5\%}$ , at 5% concentration. After that, when the resin concentration increased from 10 to 20 wt %, an additional 20% number increase was observed. An increase in the number and size of emulsified droplets with the concentration was also reported by Osborn and Akoh,<sup>16</sup> who dealt with oil-in-water emulsions. The larger the resin content, the higher the viscosity of the emulsion, as summarized in Table 1. The later finding is also consistent with the observations of Chanamai and McClements.<sup>17</sup>

**Table 1. Viscosity of the Resin–Epoxy Emulsion**

resin concentration [wt %]	5	10	20
viscosity [cP]	8600	10080	14100

**3.2. Morphology of the Core–Shell Nanofibers and the Encasing Matrix.** Figure 3a shows a nanofiber mat deposited on an aluminum foil. The SEM image of that nanofiber mat reproduced in Figure 3b shows that the nanofiber diameter is in the range of 200–300 nm when no beads were formed. The beads were formed because of capillary instability. The uniformity of nanofibers can probably be improved by increasing the electrical conductivity of the solution, which was shown, at least, for monolithic fibers electrospun from the other polymer solutions.<sup>18,19</sup> However, in the present work, no additive was used in order to keep the content of the nanofiber as pure as possible for sample analyses.

Parts c and d of Figure 3 show OM images of the solidified epoxy–resin matrix alone with no encased nanofibers for the sake of better visualization, with the encapsulated droplets containing a liquid resin monomer in the solid epoxy matrix. The solidified epoxy–resin film was prepared by drop-casting of 5 mL of the resin–epoxy solution followed by 24 h of a drying and solidification period. A deep cut was intentionally made through the solidified matrix with a razor, as is seen in Figure 3c. The figure also shows that the size of a nearby embedded resin-containing droplet highlighted by an arrow is approximately 100  $\mu\text{m}$ . These embedded resin droplets are fractured by the cut and release the resin monomer. The OM image in Figure 3d was taken 2 h after the cut was inflicted. The material surrounding the cut-line is wet and impregnated with a released resin monomer, as designed. It is worth noting that epoxy is hydrophobic when solidified. Therefore, only oil-like substances such as a resin monomer can impregnate voids/cuts in the epoxy. The released resin does not undergo polymerization and does not solidify unless it is in contact with the cure material. Because the solidified matrix in Figure 3 does not embed the cure-containing nanofibers, the resin monomer remains a liquid.

The presence of cure inside the nanofibers was confirmed by electron-dispersive X-ray (EDX) analysis. Figure 4 compares

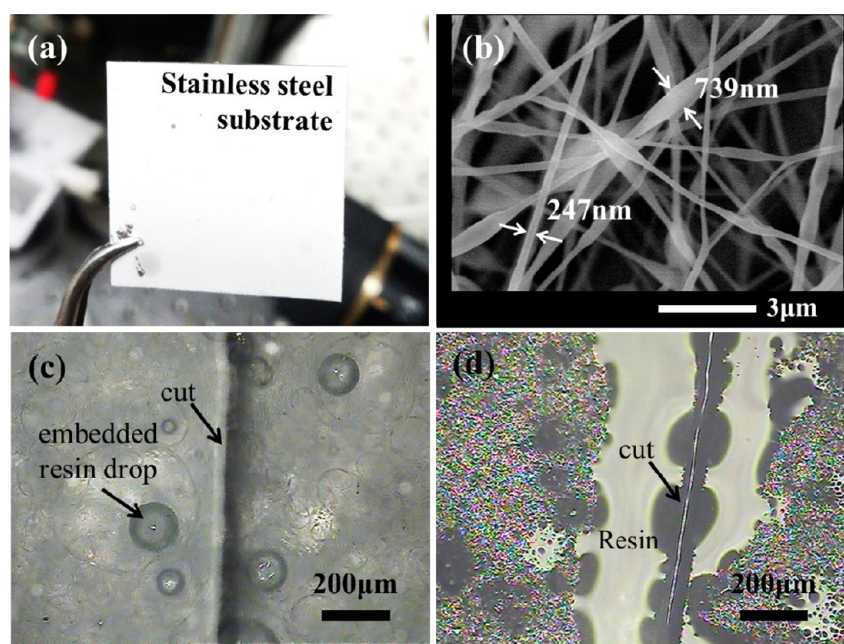


**Figure 3.** (a) Macroscopic image of a mat of core–shell nanofibers with cure encapsulated in the core. (b) SEM image of core–shell nanofibers from the mat in panel a. (c) OM image of a cut through a film of solidified epoxy with embedded resin droplets (a 20 wt % resin sample). (d) Resin released from the cut in panel c.

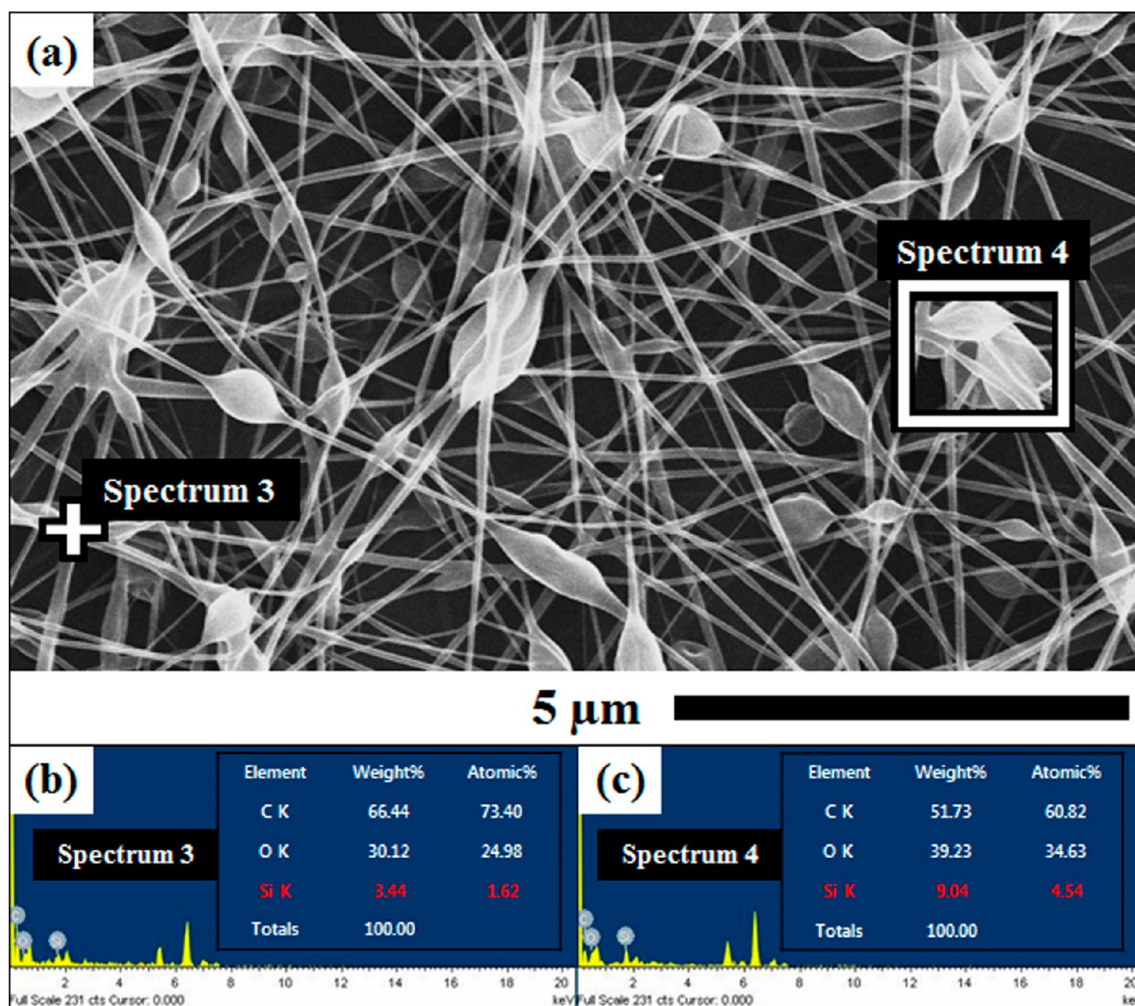


**Figure 4.** (a) SEM and (b and c) EDX data for nanofibers with the cure material in the core. Data were obtained in (b) the region of a uniform fiber, spectrum 3, and in (c) the region of the beads-on-fibers, spectrum 4.

the SEM images and EDX data for the uniform parts of the nanofibers and in the beads-on-fibers. The beads should contain more cure because they are bulky volumes with more space to store the cure material. Figure 5 confirms such larger

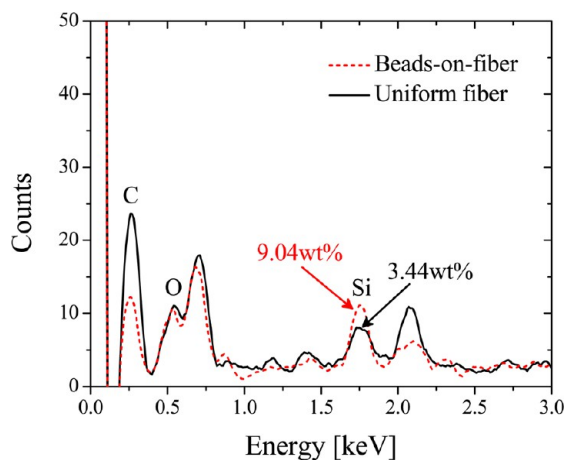


**Figure 5.** EDX data for core-shell nanofibers with the cure material in the core. A silicon peak at 1.739 keV implies the presence of cure inside the nanofibers.

storage of cure in the beads-on-fibers by comparing the silicon contents in different detection domains, spectra 3 and 4. A peak corresponding to the silicon content is higher for the beads-on-fibers. The silicon content was also detected in the uniform parts of the fibers, indicating continuous cure cores throughout these core-shell nanofibers. It should be emphasized that cure is uniformly distributed in the core of multiple long sections of nanofibers spanning these beads. Therefore, a 3D network of the nanofibers results in uniform coverage of the surface, which is difficult to achieve with the approach that involves capsules.

SEM images from Figure 6 show the view of a cut cross section of the 20 wt % epoxy-resin solidified matrix comprising the cure-containing nanofibers deposited during  $t_{\text{dep}} = 10$  min. In this case, the cut released cure, but the solidified matrix was rinsed with water immediately after the cut and, thus, no self-healing was operated for observation purposes. In particular, the presence of the embedded resin droplets was visualized as the elliptical holes, which were once occupied by the liquid resin monomer, also released by the cut. The magnified view in Figure 6b shows the ellipsoidal hole with semiaxes of about  $a = 28.13 \mu\text{m}$  and  $b = 19.2 \mu\text{m}$  for the left hole and  $a = 43 \mu\text{m}$  and  $b = 17 \mu\text{m}$  for the right hole. Note that the ellipsoidal shape resulted from the cut. The volume-equivalent radius of the cut droplet is then  $r^3 = ab^2$ , which is about  $r = 21.81$  and  $23.16 \mu\text{m}$  for the left and right holes, respectively. The average hole size is

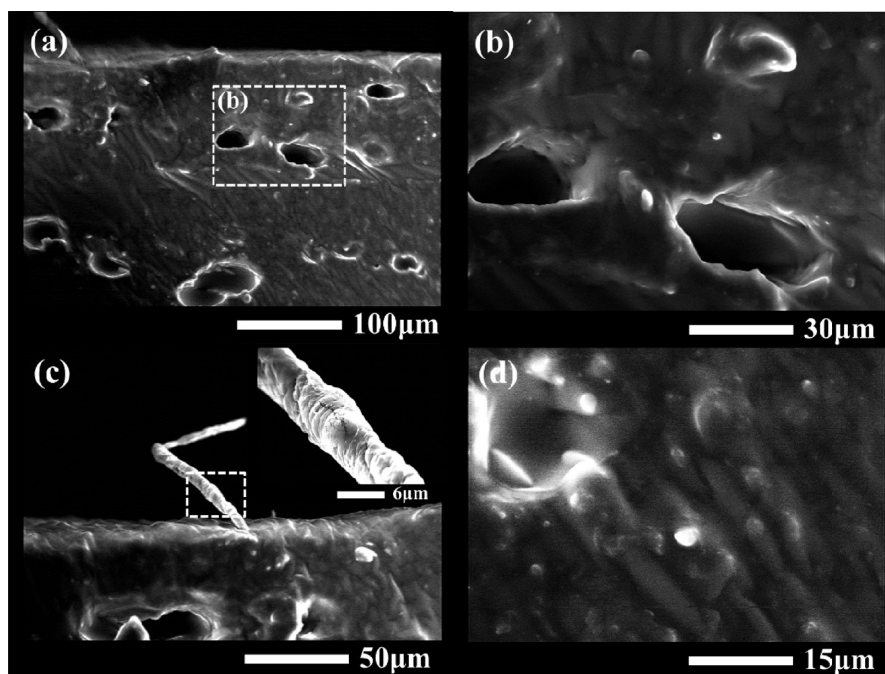


**Figure 6.** (a and c) Cross-sectional SEM image of the epoxy–resin matrix with embedded nanofibers. (b) Zoomed-in image of the area inside the box in panel a, with the volume-equivalent diameters of the two holes (cut resin droplets) being  $r = 21.81$  and  $23.16 \mu\text{m}$ , which are to be compared with the droplet average diameter in the 20 wt % emulsion  $d_{\text{avg,emulsion}} = 27 \mu\text{m}$ . (d) Nanofibers embedded in the matrix cut by the razor.

in agreement with the emulsion droplet size shown in Figure 2d. Figure 6c shows a section of a nanofiber sticking out from the matrix. It shows that occasionally some nanofibers were not fully encased by the epoxy–resin matrix, even though they were wetted by the matrix material. This is evident from the fact that this sticking-out fiber is much thicker than the original ones, about  $6\text{--}7 \mu\text{m}$  thick, as is seen in Figure 6c. Figure 6d shows an SEM image of the cut cross section of the matrix. The cross section is textured with circle marks, which are indicative of the nanofibers embedded in the epoxy–resin matrix.

**3.3. TGA and DTG.** TGA and DTG were used to show the presence of cure in the nanofibers and resin droplets in the matrix. Samples were heated in the temperature range of  $30 \text{ }^\circ\text{C} < T < 800 \text{ }^\circ\text{C}$ . Because of heating, the materials underwent sublimation, melting, evaporation, and thermal degradation, i.e., released volatiles that changed the sample weight. Accordingly, TGA data show the weight loss, while DTG data show the derivative of the weight loss with respect to temperature, providing distinctive peaks corresponding to substantial volatile release.

Figure 7a shows the weight loss of pure epoxy, a core–shell nanofiber mat with cure in the core, and epoxy–resin matrices with a resin concentration of 20 wt %. Note that the nanofiber deposition time was  $t_{\text{dep}} = 10 \text{ min}$  for the samples in Figure 7. Figure 7b shows the corresponding DTG data. There is a sharp peak at  $400.2 \text{ }^\circ\text{C}$ , which corresponds to the boiling temperature of pure epoxy. On the other hand, epoxy–resin matrices at 20 wt % resin show strong peaks at about  $416 \text{ }^\circ\text{C}$ , shifted by  $16 \text{ }^\circ\text{C}$  from pure epoxy. The peak for the 20 wt % matrix containing resin is clearly pronounced. It should be emphasized that this matrix also contained the embedded nanofibers.

The peak at  $176.1 \text{ }^\circ\text{C}$  produced by the nanofiber mat corresponds to the cure, which is substantiated by a clearly distinct peak at about  $305 \text{ }^\circ\text{C}$  corresponding to PAN. Indeed,  $176.1 \text{ }^\circ\text{C}$  is the boiling temperature of the cure. The 5 and 20

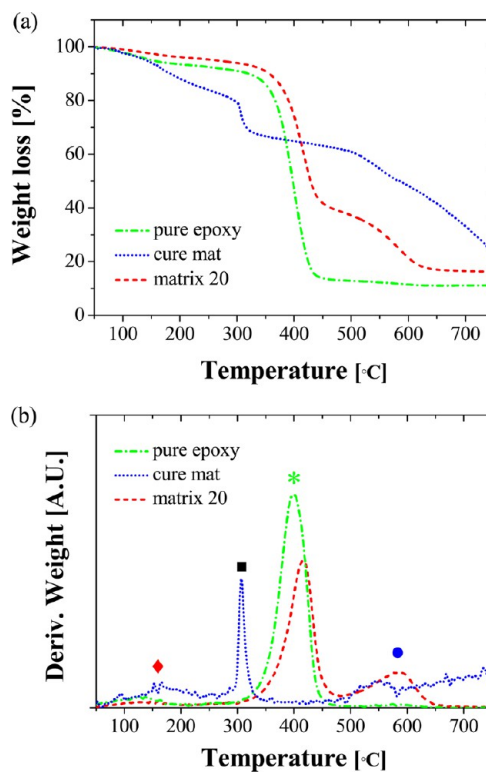


**Figure 7.** (a) TGA results. (b) Corresponding DTG results. (red  $\blacklozenge$ , cure,  $176.1 \text{ }^\circ\text{C}$ ; black  $\blacksquare$ , PAN,  $305.0 \text{ }^\circ\text{C}$ ; light-green  $*$ , epoxy–resin matrices with 20 wt % resin,  $416.1 \text{ }^\circ\text{C}$ ; blue  $\bullet$ , resin,  $576.3 \text{ }^\circ\text{C}$ ). Note that “matrix 20” herein refers to epoxy–resin matrices with 20 wt % resin. The nanofiber mat with cure in the fiber core is denoted as “cure mat” herein.

wt % matrices also incorporated nanofibers with cure in the core; i.e., they were composite self-healing materials. Therefore,

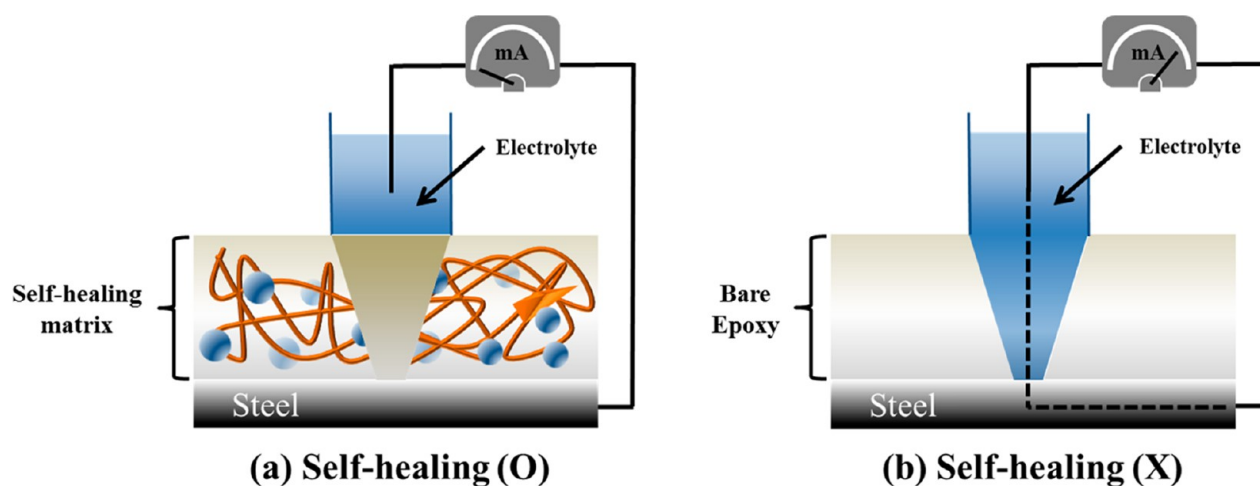


**Figure 8.** Schematic of the electrochemical test: (a) self-healing material embedded case; (b) control case. This experiment is an electrochemical analogue of SVET.

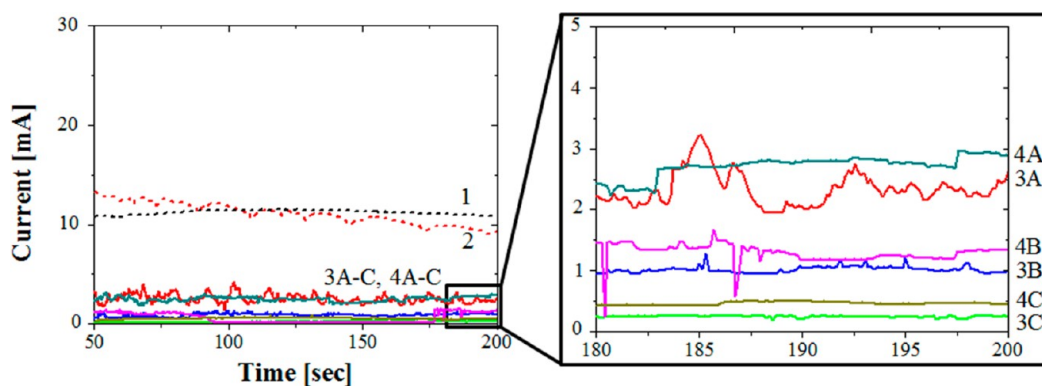


**Figure 9.** Electric current: (1) epoxy; (2) resin–epoxy (5 wt %); (3A) cure mat 3 min, matrix 5; (3B) cure mat 3 min, matrix 10; (3C) cure mat 3 min, matrix 20; (4A) cure mat 10 min, matrix 5; (4B) cure mat 10 min, matrix 10; (4C) cure mat 10 min, matrix 20. Time is reckoned from the moment when measurements have been started.

the peak at 176.1 °C should also be present in the data for the matrices. The magnification of the DTG data for these matrices near 176.1 °C shows the weak peaks, which confirms the presence of cure in the composite material. The DTG data for the matrices near 305 °C were difficult to resolve because of the relatively small amount of PAN. Last, the boiling temperature of the resin in the matrices is 576.3 °C. At the resin concentration of 5 wt %, confirmation of the resin peak was indeterminate as no distinctive peak, but a round peak was present (not shown). However, the resin peak at 576.3 °C is clearly visible at 20 wt % resin in the matrix.

**3.4. Self-Healing Test.** Often, a self-healing layer is transparent, and thus visible confirmation of self-healing is possible by prevention of corrosion of the underlying metal substrate by the self-healing coating. However, in the present case, the self-healing composite is not transparent (see Figure S1 in the Supporting Information), and thus an alternative means of confirming the self-healing is required.

To test the self-healing capability of the composite, an electrochemical device was designed, as depicted in Figure 8, which is an electrochemical analogue of SVET. The self-healing composite coating was prepared on top of the stainless steel substrate. The substrate and coating are in contact with a layer of an electrolyte and included in the electric circuit. However, with the coating being intact, there is no electric current in the circuit because the coating is an isolator. Once a cut is made to

the coating, the bottom stainless steel is exposed to the electrolyte and the electric current in the circuit becomes possible. At the same time, the resin monomer and cure being liquid are released from the fractured droplets and nanofiber cores, respectively, to the damaged area. Once resin and cure are combined, the resin undergoes a cross-linking reaction and solidifies, which manifests the coating self-healing and would cut the current off once again.

Coatings were cut by a razor and left for a 48 h resting time to allow cross-linking and polymerization of resin and cure. Then the electric current was measured as described above in conjunction with Figure 8. Figure 9 shows the measured electrical current versus time. In the non-self-healing cases (i.e., epoxy and resin–epoxy cases), an electrical current of about 10 mA was measured for 200 s. This is a clear manifestation that these coatings have not self-healed, as expected. On the other hand, the self-healing coatings (i.e., matrices 5, 10, and 20 for both  $t_{\text{dep}} = 3$  and 10 min) revealed an electrical current below 2.5 mA (comparable to the noise level), which is effectively an insulation case, which means that these coatings underwent self-healing. This happened for coatings deposited with  $t_{\text{dep}} = 3$  or 10 min, which indicates that  $t_{\text{dep}}$  does not play a critical role in the self-healing performance. It means that the lengthy deposition time for producing cure nanofibers is not necessary, which is a favorable fact from the manufacturing point of view. The signals below the noise levels also do not allow one to

distinguish reliably the effect of the resin content (i.e., matrix 5 vs matrix 20 cases) but imply that a larger resin content with respect to the amount of cure is preferable in order to maximize the self-healing performance.

#### 4. CONCLUSION

Electrospinning of emulsions of the cure material DMHS in a PAN solution in DMF results in core-shell nanofibers with cure in the core and PAN in the shell. This is proven by SEM, EDX, TGA, and DTG. The presence of liquid droplets of a dimethylvinyl-terminated DMS resin monomer in the encasing epoxy matrix is revealed by means of SEM, TGA, and DTG. By direct measurements of the electric current through cuts on damaged coatings, it is shown that they self-heal. This means that the self-healing coatings practically eliminate the electric current through the original cut because the resin monomer released from droplets in the damaged matrix is polymerized in the presence of the cure released from the damaged nanofibers. The self-healing demonstrated in this work is applicable to slow microcracking due to fatigue rather than catastrophic crack propagation. It should be emphasized that in the present work we focused on the self-healing for anticorrosion protection. This is a different feature than self-healing for mechanical strength recovery. Whether the same coating (or any other coating of this type) could also recover mechanical strength in the case of material fatigue or delamination is currently an open question that deserves further study.

#### ■ ASSOCIATED CONTENT

##### Supporting Information

Light transmittance at different wavelengths. This material is available free of charge via the Internet at <http://pubs.acs.org>.

#### ■ AUTHOR INFORMATION

##### Corresponding Authors

\*E-mail: [ayarin@uic.edu](mailto:ayarin@uic.edu).

\*E-mail: [skymoon@korea.ac.kr](mailto:skymoon@korea.ac.kr).

##### Author Contributions

‡Equal contribution.

##### Notes

The authors declare no competing financial interest.

#### ■ ACKNOWLEDGMENTS

This work was supported by the Human Resources Development program (No. 20124030200120) of the Korea Institute of Energy Technology Evaluation and Planning (KETEP) and by the Industrial Strategic Technology Development Program (MKE-10045221).

#### ■ REFERENCES

- (1) Ramakrishna, S.; Mayer, J.; Wintermantel, E.; Leong, K. W. Biomedical Applications of Polymer-composite Materials: A Review. *Compos. Sci. Technol.* **2001**, *61*, 1189–1224.
- (2) Rawal, S. Metal-Matrix Composites for Space Applications. *JOM* **2001**, *53*, 14–17.
- (3) Asnafi, N.; Langstedt, G.; Andersson, C.-H.; Ostergren, N.; Hakansson, T. A New Lightweight Metal-composite-metal Panel for Applications in the Automotive and Other Industries. *Thin-Walled Struct.* **2000**, *36*, 289–310.
- (4) White, S. R.; Sottos, N. R.; Geubelle, P. H.; Moore, J. S.; Kessler, M. R.; Sriram, S. R.; Brown, E. N.; Viswanathan, S. Autonomic Healing of Polymer Composites. *Nature* **2001**, *409*, 794–797.

(5) Kim, G. B.; Lim, N. Y.; Lee, S. J. Hollow Microcapsules for Sensing Microscale Flow Motion in X-ray Imaging Method. *Microfluid. Nanofluid.* **2009**, *6*, 419–424.

(6) Keller, M. W.; White, S. R.; Sottos, N. R. A Self-Healing Poly(Dimethyl Siloxane) Elastomer. *Adv. Mater.* **2007**, *17*, 2399–2404.

(7) Cho, S. H.; Andersson, H. M.; White, S. R.; Sottos, N. R.; Braun, P. V. Polydimethylsiloxane-Based Self-Healing Materials. *Adv. Mater.* **2006**, *18*, 997–1000.

(8) Cho, S. H.; White, S. R.; Braun, P. V. Self-Healing Polymer Coatings. *Adv. Mater.* **2009**, *21*, 645–649.

(9) Lee, M. W.; An, S.; Lee, C.; Liou, M.; Yarin, A. L.; Yoon, S. S. Self-healing Transparent Core-shell Nanofiber Coatings for Anti-corrosive Protection. *J. Mater. Chem. A* **2014**, *2*, 7045–7053.

(10) Shchukin, D. G.; Zheludkevich, M.; Yasakau, K.; Lamaka, S.; Ferreira, M. G. S.; Mõhwald, H. Layer-by-Layer Assembled Nanocontainers for Self-Healing Corrosion Protection. *Adv. Mater.* **2006**, *18*, 1672–1678.

(11) Shchukin, D. G.; Mchwald, H. Self-Repairing Coatings Containing Active Nanoreservoirs. *Small* **2007**, *3*, 926–943.

(12) Li, Q.; Mishra, A. K.; Kim, N. H.; Kuila, T.; Lau, K.-t.; Lee, J. H. Effects of Processing Conditions of Poly(methylmethacrylate) Encapsulated Liquid Curing Agent on the Properties of Self-healing Composites. *Composites: Part B* **2013**, *49*, 6–15.

(13) Mata, A.; Fleischman, A. J.; Roy, S. Characterization of Polydimethylsiloxane (PDMS) Properties for Biomedical Micro/Nanosystems. *Biomed. Microdevices* **2005**, *7*, 281–293.

(14) Bazilevsky, A. V.; Yarin, A. L.; Megaridis, C. M. Co-electrospinning of Core-Shell Fibers Using a Single-Nozzle Technique. *Langmuir* **2007**, *23*, 2311–2314.

(15) Yarin, A. L. Coaxial Electrospinning and Emulsion Electrospinning of Core-shell Fibers. *Polym. Adv. Technol.* **2011**, *22*, 310–317.

(16) Osborn, H. T.; Akoh, C. C. Effect of Emulsifier Type, Droplet Size, and Oil Concentration on Lipid Oxidation in Structured Lipid-based Oil-in-water Emulsions. *Food Chem.* **2004**, *84*, 451–456.

(17) Chanamai, R.; McClements, D. J. Dependence of Creaming and Rheology of Monodisperse Oil-in-water Emulsions on Droplet Size and Concentration. *Colloids Surf., A* **2000**, *172*, 79–86.

(18) Lee, M. W.; An, S.; Latthe, S. S.; Lee, C.; Hong, S.; Yoon, S. S. Electrospun Polystyrene Nanofiber Membrane with Superhydrophobicity and Superoleophilicity for Selective Separation of Water and Low Viscous Oil. *ACS Appl. Mater. Interfaces* **2013**, *5*, 10597–10604.

(19) Lee, M. W.; An, S.; Joshi, B.; Latthe, S. S.; Yoon, S. S. Highly Efficient Wettability Control via Three-Dimensional (3D) Suspension of Titania Nanoparticles in Polystyrene Nanofibers. *ACS Appl. Mater. Interfaces* **2013**, *5*, 1232–1239.